Available online at www.sciencedirect.com
SCIENCE DIRECT®
International Journal of Multiphase Flow 31 (2005) 843–866
International Journal of Multiphase Flow
www.elsevier.com/locate/ijmulflow

Direct numerical simulation of a particle-laden mixing layer with a chemical reaction

Takenobu Michioka [a,*], Ryoichi Kurose [b,1], Kouichi Sada [a], Hisao Makino [b]

[a] *Environmental Science Research Laboratory, Central Research Institute of Electric Power Industry (CRIEPI), Chiba 270-1194, Japan*

[b] *Energy Engineering Research Laboratory, Central Research Institute of Electric Power Industry (CRIEPI), Yokosuka, Kanagawa 240-0196, Japan*

Received 3 September 2004; received in revised form 10 December 2004

Abstract

A direct numerical simulation (DNS) is applied to a particle-laden turbulent mixing layer with a chemical reaction, and the effects of particles on turbulence and chemical species' diffusion and reaction in both zero and finite gravity cases are investigated. Unreactive particles, whose response time, τ_P, is smaller than the Kolmogorov time scale, τ_K [$\tau_P/\tau_K = O(10^{-1})$], are uniformly injected into the high-speed side of the mixing layer. Two reactive chemical species are separately introduced through different sides. The results show that although laden particles generally depress turbulent intensities, they begin to enhance turbulent intensities downstream as the particle size decreases provided that the inlet particle volume fraction is fixed. This is because that the small particles with small particle response time easily accumulate at the circumference of coherent vortices and act to suppress the growth of primitive small-scale coherent vortices upstream but enhance that of relatively developing large-scale ones downstream. Also, since the small-scale turbulence, which promotes the chemical reaction, is suppressed by the laden particles in the entire region, chemical product decreases overall. Furthermore, the presence of finite gravity on the particles acts to depress the turbulent intensities, but its effects on chemical species' diffusion and reaction are quite small.

* Corresponding author. Tel.: +81 4 7182 1181; fax: +81 4 7183 2966.
E-mail address: michioka@crieipi.denken.or.jp (T. Michioka).
[1] Present address: Center for Turbulence Research, Stanford University, Stanford, CA 94305-3035, USA.

0301-9322/$ - see front matter © 2005 Elsevier Ltd. All rights reserved.
doi:10.1016/j.ijmultiphaseflow.2005.03.006

Keywords: Two-phase turbulence; Mixing layer; Direct numerical simulation; Chemical reaction; Finite gravity

1. Introduction

Particle-laden turbulent flows with chemical reactions are encountered in atmospheric environment and in a number of engineering applications such as energy conversion and propulsive devices using solid or liquid fuels. It is therefore of great importance to understand the effects of the laden particles on turbulence and chemical species' diffusion and reaction in turbulent reacting flows.

With the advantage of powerful supercomputers, numerical simulations such as direct numerical simulation (DNS) and large-eddy simulation (LES), have become a viable tool for investigating particle-laden turbulent flows with chemical reactions (Mashayek, 2000; Glaze and Frankel, 2000; Kurose and Makino, 2003). For simulating the particle-laden turbulent flows with these methods, the particle–particle interactions and turbulent modulation by particles are significant. However, in most practical particle-laden turbulent flows, the volume fraction of the dispersed particle is small, so that particle–particle interactions are often negligible. On the other hand, the particle mass volume fraction often becomes large owing to a large density ratio of solid particle to air, so that the modulation of turbulence by particles cannot be neglected and two-way coupled simulation including momentum exchange between them must be implemented (Elghobashi, 1991, 1994).

Squires and Eaton (1990), Elghobashi and Truesdell (1993), Boivin et al. (1998) and Sundaram and Collins (1999) performed the two-way coupled DNS of isotropic turbulence with solid particles, whose response time, τ_P, is larger than the Kolmogorov time scale, τ_K, and found that the particles with $\tau_P \geqslant \tau_K$ reduce the turbulent kinetic energy (turbulent intensities). Yamamoto et al. (2001) performed two-way coupled LES of the turbulent gas–particle flow in a vertical channel, and showed that the particles with $\tau_P \geqslant \tau_K$ decrease the turbulent intensities. On the other hand, Druzhinin (2001) performed the two-way coupled DNS of isotropic turbulence under the condition of $\tau_P < \tau_K$, and showed that the particles enhance the kinetic energy (turbulent intensities), which is in contrast to the reduction of turbulent intensities by particles with $\tau_P \geqslant \tau_K$. A similar result was also obtained by Ahmed and Elghobashi (2000) for two-way coupled DNS of turbulent homogeneous shear flows with dispersed particles. Thus, it is known that in the homogeneous flows, the laden particles with $\tau_P \geqslant \tau_K$ and $\tau_P < \tau_K$ tend to depress and enhance the turbulent intensities, respectively.

However, the above previous studies were performed only for fully developed homogeneous turbulent flows, and the number of studies for inhomogeneous turbulent flows such as a spatially developed mixing layer and a jet, in which the physical mechanisms of turbulent modulation may change with the streamwise distance, is small. Yuu et al. (1996) performed two-way coupled DNS of a turbulent jet, and showed that the particles with $\tau_P \geqslant \tau_K$ decrease the turbulent intensities. Yang et al. (1990) and Dimas and Kiger (1998) investigated the stability of two-way coupled mixing layers with uniformly distributed particles by linear stability analysis under the condition of $\tau_P \geqslant \tau_K$, and showed that the presence of the particles enhances the stability of the flows and decreases the amplification rate of perturbations in the flow. However, the influence of particles with

$\tau_P < \tau_K$ on turbulence has not been studied. Furthermore, though effects of laden particles on the chemical species' diffusion and reaction (Mashayek, 2000; Reveillon and Vervisch, 2000) and the role of finite gravity (Wang and Maxey, 1993; Meiburg et al., 2000; Ferrante and Elghobashi, 2003) has been investigated in many studies, no one has discussed them in any spatially developing particle-laden flows in detail.

The purpose of this study is to investigate the effects of laden particles with $\tau_P < \tau_K$ on turbulence and chemical species' diffusion and reaction in a spatially developing turbulent mixing layer. The influences of finite gravity acting on particles on turbulent modulation and scalar behavior are also discussed. The direct numerical simulation (DNS) is performed for the particle-laden turbulent mixing layer with a chemical reaction, in both zero and finite gravity conditions. Unreactive particles, whose response time is smaller than the Kolmogorov time scale, $\tau_P/\tau_K = O(10^{-1})$, are uniformly injected into the high-speed side, and the particle trajectories are individually pursued in a Lagrangian method. Two chemical species are separately introduced through different sides, and a second-order, irreversible and isothermal reaction between them is assumed to take place in the region along the central interface.

The paper is organized as follows. In Section 2, the governing equations for continuous and dispersed phases and computational details are described. The results are presented in Section 3. The effects of particle response time on turbulence and chemical species' diffusion and reaction under the zero gravity condition are discussed in Sections 3.1 and 3.2, respectively. The effect of particle volume fraction is also studied under the zero gravity condition in Section 3.3. In Section 3.4, the effects of finite gravity acting on particles on turbulence and chemical species' diffusion and reaction are discussed. A summary of the findings of this paper is presented in Section 4.

2. Direct numerical simulation

2.1. Governing equations for continuous phase

The governing equations for particle-laden turbulent flow with a chemical reaction are continuity, momentum (Navier–Stokes, N–S) and mass conservation equations and are written as

$$\frac{\partial U_i}{\partial x_i} = 0, \tag{1}$$

$$\frac{\partial U_i}{\partial t} + \frac{\partial U_j U_i}{\partial x_j} = -\frac{\partial P}{\partial x_i} + \frac{1}{Re}\frac{\partial^2 U_i}{\partial x_j \partial x_j} + \Psi_{u_i}, \tag{2}$$

$$\frac{\partial \Gamma_i}{\partial t} + \frac{\partial U_j \Gamma_i}{\partial x_j} = \frac{1}{Re\,Sc}\frac{\partial^2 \Gamma_i}{\partial x_j \partial x_j} + \omega, \tag{3}$$

where U_i, Γ_i and P are instantaneous velocity of i component, instantaneous concentration of chemical species i and instantaneous pressure, respectively. These equations are non-dimensionalized using the vertical computational length, $L^* = 0.05$ m, velocity difference between inlet high-speed side and lower-speed side, $\Delta U^* = 2.5$ m/s, fluid density, $\rho_f^* = 1.2$ kg/m^3, viscosity, $\mu^* = 1.8 \times 10^{-5}$ Pa s, and initial concentration of species A, C_{A0}^*. When a second-order, irreversible

and isothermal reaction (A + B → P) is considered, the chemical reaction source term is expressed as

$$\omega = \begin{cases} -Da\Gamma_{\mathrm{A}}\Gamma_{\mathrm{B}} & (i = 1, 2 \text{ in Eq. (3)}) \\ Da\Gamma_{\mathrm{A}}\Gamma_{\mathrm{B}} & (i = 3 \text{ in Eq. (3)}). \end{cases} \tag{4}$$

The Reynolds number, Re, Schmidt number, Sc, and Damköhler number, Da, are defined as

$$Re = \frac{\rho_{\mathrm{f}}^* \Delta U^* L^*}{\mu^*}, \tag{5}$$

$$Sc = \frac{\mu^*}{\rho_{\mathrm{f}}^* D^*}, \tag{6}$$

$$Da = \frac{k_{\mathrm{r}}^* L^* C_{\mathrm{A0}}^*}{\Delta U^*}, \tag{7}$$

where D^* is molecular diffusivity of mass and k_{r}^* is chemical reaction constant.

Ψ_{u_i} in Eq. (2) is the momentum exchange between the continuous and dispersed phases, which is considered by the particle-source-in-cell (PSI-Cell) method (Crowe et al., 1977) and is expressed as

$$\Psi_{u_i} = -\frac{1}{\delta_{\mathrm{c}}} \sum^{n_{\mathrm{c}}} \frac{m_{\mathrm{p}} \Phi}{\tau_{\mathrm{p}}} (U_i - U_{\mathrm{p},i}), \tag{8}$$

where $U_{\mathrm{p},i}$ is the particle velocity of particle number i, δ_{c} is the cell volume ($\delta_{\mathrm{c}} = \Delta_1\Delta_2\Delta_3$, Δ_i is the width of the computational grid) and n_{c} is the number of solid particles within the volume of the grid. Φ is shown later.

2.2. Governing equation for dispersed phase

The solid particles are tracked individually in a Lagrangian manner. It is assumed that the particle material density is much larger than the fluid density, $\rho_{\mathrm{P}} \gg \rho_{\mathrm{F}}$, such that the dominating forces acting on the particle by the surrounding fluid are the drag and lift, and other forces (the pressure gradient, added mass, and Basset) can be neglected.

The non-dimensional Lagrangian particle equations are given as,

$$\frac{\mathrm{d}x_{\mathrm{p},i}}{\mathrm{d}t} = U_{\mathrm{p}.i}, \tag{9}$$

$$\frac{\mathrm{d}U_{\mathrm{p},i}}{\mathrm{d}t} = F_{\mathrm{D}} + F_{\mathrm{L}} + \frac{1}{F_{\mathrm{r}}^2} e_g, \tag{10}$$

where F_{D} and F_{L} are the drag and lift forces, respectively. Finite gravity has the magnitude g in the direction e_g. The Froud number is defined as

$$F_{\mathrm{r}} = \frac{\Delta U^*}{\sqrt{L^* g}}. \tag{11}$$

The drag force, F_D, is written as

$$F_D = -\frac{1}{\tau_P}(U_{P,i} - U_i)\Phi. \tag{12}$$

Here, τ_P, which is referred to as the particle response time, is defined by

$$\tau_p = \frac{d_P^2 \rho_P Re}{18\mu}, \tag{13}$$

where Φ (Glaze and Frankel, 2000) is given as

$$\Phi = \begin{cases} 1 + \frac{3}{16} Re_p & (Re_p \leqslant 0.01), \\ 1 + 0.1315 Re_p^{(0.82 - 0.05w)} & (0.01 \leqslant Re_p \leqslant 20) \end{cases}, \tag{14}$$

with

$$w = \log_{10} Re_p.$$

Here, Re_p is the particle Reynolds number based on the particle diameter, d_p, and the relative velocity between the particle and fluid:

$$Re_p = \frac{d_P |U_{p,i} - U_i| \rho_f}{\mu} Re. \tag{15}$$

Regarding the lift force, Mei's expression (Mei, 1992) is employed. This equation is

$$F_L = 0.443 J(\varepsilon) F_L^S. \tag{16}$$

Here, the superscript 'S' means the value given by Saffman's expression (Saffman, 1965).

$$F_L^S = -6.168 \frac{\rho_f}{\rho_P} \frac{1}{d_p^2} (U_P - U_f) \sqrt{\frac{1}{Re} \frac{dU}{dy}}. \tag{17}$$

The non-dimensional quantity J in Eq. (16) is given by

$$J(\varepsilon) \approx 0.6765\{1 + \tanh[2.5 \log_{10}(\varepsilon + 0.191)]\}\{0.667 + \tanh[6(\varepsilon - 0.32)]\}, \tag{18}$$

$$\varepsilon = \frac{\sqrt{Re_\alpha}}{Re_p} = \frac{1}{Re_p} \sqrt{Re \frac{\rho_f d_p^2}{\upsilon} \frac{dU}{dy}}. \tag{19}$$

The validity of this equation was verified by Kurose and Komori (1999) for $R_{ep} < 10$. The effect of particle rotation on the fluid force acting on the particles is neglected owing to small R_{ep} (Kurose and Komori, 1999).

2.3. Computational details

Fig. 1 shows the schematic of the computational domain. The non-dimensional computational domain was $6 \times 1 \times 1$ in the streamwise (x), vertical (y) and spanwise (z) directions. The origin of the co-ordinate axes x, y and z was set at the center of the inlet boundary. Solid particles were injected uniformly into the high-speed side of the mixing layer, and the reactive chemical species

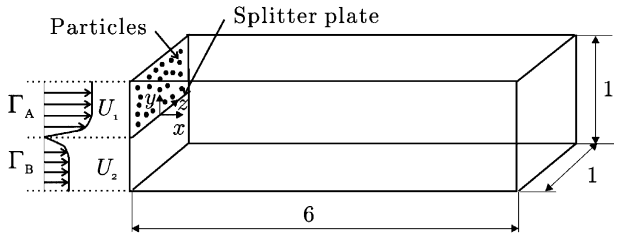

Fig. 1. Schematic of computational domain.

A and B were provided separately in the high- and low-speed sides. The high- and low-speed free-stream velocities were $U_h = 2.0$ and $U_l = 1.0$, respectively. The Reynolds number, *Re*, defined by Eq. (5) was 8333 and the Schmidt number, *Sc*, defined by Eq. (6) was 1.0 because of an air flow. The Damköhler number, *Da*, defined by Eq. (7) was 1.0 under the assumption that the reaction between the reactive chemical species A and B takes place at a moderately fast reaction rate (Michioka and Komori, 2004).

The initial random perturbation, u_i, was given in the sinusoidal form:

$$u_i(x,y,z) = \sum_{n=1}^{20} u_i''(y)\sin(2\pi n f_0 x + \theta_i(x,y,z,nf_0)), \tag{20}$$

$$U_i(x,y,z) = \overline{U_i}(x,y,z) + u_i(x,y,z), \tag{21}$$

where $u_i''(y)$ is the rms value of the turbulence intensity, f_0 is the basic frequency of 0.2 and θ_i is the uniformly distributed random number between 0 and 1. The vertical distributions of the time-averaged velocity, $\overline{U_i}$, and $u_i''(y)$ were given by the DNS data of Spalart (1988). Slip boundary conditions were imposed on the velocity components on the upper and lower walls. Periodic boundary conditions were imposed on the velocity and scalar component in the spanwise direction. Convective boundary conditions ($\partial U_i/\partial t + \overline{U}\cdot\partial U_i/\partial x = 0$) were applied at the exit of the domain. This condition avoids the problem caused by pressure perturbations being reflected of the outflow boundary back to the computational domain (Ferziger and Peric, 2002). The detailed

Table 1
Particle properties (dimensionless)

Run no.	d_p	τ_P	d_P/η	τ_P/τ_K	ϕ_{v0}	v_t
RUN I	–	–	–	–	0.0	–
RUN II	5.0×10^{-3}	0.115	0.046	0.12	2.62×10^{-4}	0
RUN III	8.0×10^{-3}	0.296	0.073	0.30	2.62×10^{-4}	0
RUN IV	1.25×10^{-2}	0.725	0.12	0.50	2.62×10^{-4}	0
RUN V	5.0×10^{-3}	0.115	0.046	0.12	1.68×10^{-5}	0
RUN VI	5.0×10^{-3}	0.115	0.046	0.12	1.07×10^{-3}	0
RUN IIG	5.0×10^{-3}	0.115	0.046	0.12	2.62×10^{-4}	9.02×10^{-3}
RUN IIIG	8.0×10^{-3}	0.296	0.073	0.30	2.62×10^{-4}	2.32×10^{-2}
RUN IVG	1.25×10^{-2}	0.725	0.12	0.50	2.62×10^{-4}	5.68×10^{-2}

All variables are nondimensionalized by the representative length (vertical computational length), $L^* = 0.05$ m, the velocity difference, $\Delta U^* = 2.5$ m/s, fluid density, $\rho^* = 1.2$ kg/m^3 and viscosity, $\mu^* = 1.8\times10^{-5}$ Pa s.

particle properties are listed in Table 1. RUNs II–IV have the same particle volume fraction of $\phi_{v0} = 2.62 \times 10^{-4}$ at the inlet of the high-speed side of the mixing layer, and the ratio of the particle response time to the Kolmogorov time scale, τ_P/τ_K, ranges from 0.12 to 0.50 (RUN I is the particle-free case). RUNs II, V and VI have ϕ_{v0} ranging from 1.68×10^{-5} to 1.07×10^{-3} with the same τ_P/τ_K of 0.12. For RUNs IIG–IVG, finite gravity was imposed in $-y$ direction provided that the other conditions are the same as those for RUNs II–IV. The terminal velocities of these particles for RUNs IIG–IVG, v_t, are 9.02×10^{-3}, 2.32×10^{-2} and 5.68×10^{-2}, respectively. The non-dimensional density, ρ_P^*/ρ_F^*, was 1000. The particle–particle interactions are generally neglected under the condition of solid volume fraction, $\phi_v < O(10^{-3})$, because the models (Yonemura et al., 1973; Yamamoto et al., 2001) for particle–particle interactions require very high computational costs. Though the particle volume fraction for RUN VI is slightly larger than 1.0×10^{-3}, we neglected the particle–particle interactions for comparisons with other cases. The particle response time, τ_P, corresponds to the Stokes number, St. The Kolmogorov time scale, τ_K, and length scale, η, at $x = 3.0$ were 0.985, 1.09×10^{-4}, respectively (these values were almost constant in the entire region).

The governing equations of Eqs. (1)–(3) were discretized on a staggard mesh arrangement to construct a fully consistent and conservative finite-difference formation. The spatial derivatives in these equations were approximated by a second-order central difference scheme. However, a flux corrected transport (FCT) scheme (Boris and Book, 1973; Book et al., 1975; Boris and Book, 1976; Michioka et al., 2003) was applied to the convection term in the mass conserved equations, since the second-order central difference scheme produces a negative concentration. The Fractional step method (Kim and Moin, 1985) was used to solve the N–S equation. The time integrations of Eqs. (2), (3) and (10) were carried out by a second-order Runge–Kutta method. The numbers of the DNS grid points used here were $300 \times 100 \times 100$ in streamwise, vertical and spanwise directions. To implement the DNS, the computational grid size must be smaller than the smallest length scale (Kolmogorv scale, η) and the smallest concentration scale (the Bachelor scale, η_B). In the present DNS, the Bachelor scale is equal to the Kolmogorv length scale because of $Sc = 1$. The grid size was smaller than these scales of 1.09×10^{-4}, which was estimated using the power spectrum at $x = 3$. The time step, Δt, was set to 5.0×10^{-4}, which is quite smaller than the particle response time.

Simulations were run 60,000 time steps (20,000 time steps for initial transients, 40,000 time steps for statistics). The CPU time required for each case was approximately 216 CPU hours on a Fujitsu VPP5000 super computer.

3. Results and discussion

3.1. Effect of particle response time on turbulence (zero gravity condition)

First, the effect of particle response time, τ_P, on turbulence is investigated under the zero gravity condition. As shown in Table 1, RUNs II–IV have the same particle volume fraction of $\phi_{v0} = 2.62 \times 10^{-4}$ at the inlet of the high-speed side of the mixing layer, and the ratio of the particle response time to the Kolmogorov time scale, τ_P/τ_K, ranges from 0.12 to 0.50 (RUN I is the particle-free case).

Fig. 2 shows the instantaneous particle distributions superimposed on spanwise vorticity in (x,y)-plane for RUNs I–IV. The gray plots represent particles. Since RUN I is the particle-free case, the gray plots are not shown in Fig. 2(a). As τ_P/τ_K decreases, the particle response time, τ_P, approaches to the flow vortex time scale and the particles apparently tend to accumulate near the circumference of coherent spanwise vortices generated around the central interface (Ling et al., 1998). This is believed to be due to the fact that the particles with smaller τ_P/τ_K are easily shifted by the centrifugal effect of the spanwise vortices (Hishida et al., 1992; Ishima et al., 1993; Fan et al., 2001). It is also observed in Fig. 2 that for smaller τ_P/τ_K the development of coherent vortices is delayed but the only spanwise coherent vortices become large, particularly in the downstream region. The evolution of these spanwise coherent vortices can be quantified by that of time-averaged momentum thickness. Fig. 3 shows the streamwise distributions of the time-averaged momentum thickness. The time-averaged momentum thickness, θ, is defined as,

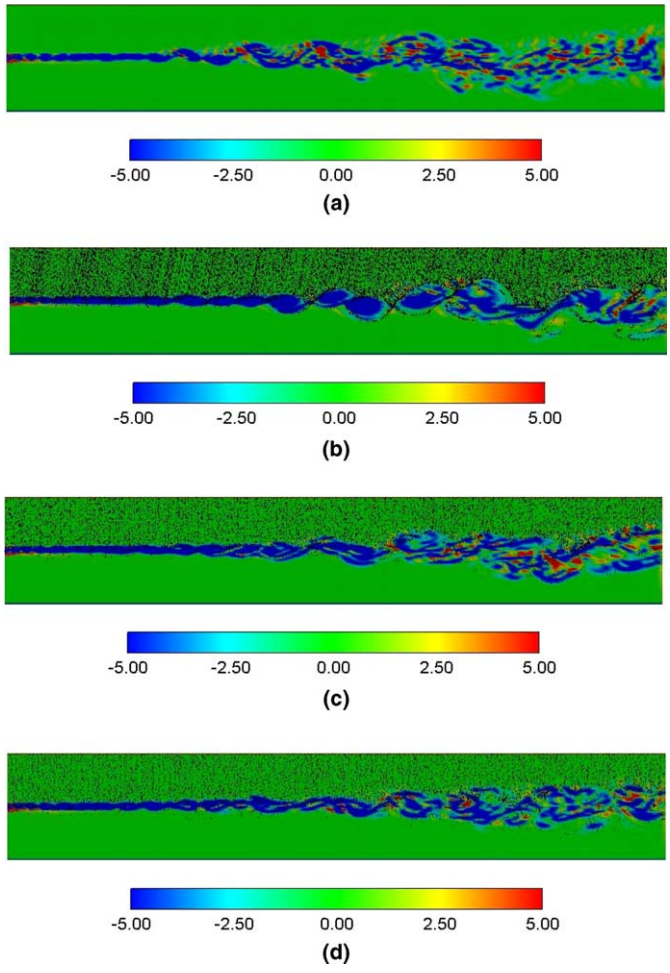

Fig. 2. Instantaneous particle distributions superimposed on spanwise vorticity in (x,y)-plane for: (a) RUN I; (b) RUN II; (c) RUN III and (d) RUN IV. The gray plots represent particles.

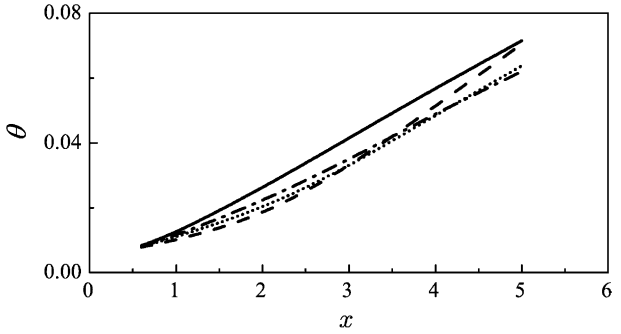

Fig. 3. Streamwise distributions of time-averaged momentum thickness, θ: (———) RUNI; (– – – –) RUN II; (·····) RUN III; (–·–·–) RUN IV.

$$\theta = \frac{1}{\Delta U^2}\int_{-0.5}^{+0.5}(U_h - \overline{U})(\overline{U} - U_l)\mathrm{d}y. \tag{22}$$

In the present mixing layer, since initial conditions of time-averaged velocities in upper- and lower sides of the mixing layer were given using the DNS data of a boundary layers, the wake appears in the region of $x < 0.6$, and the vertical distributions of the time-averaged streamwise velocity were fully developed downstream of $x = 0.6$. Because the turbulent statistics at the wake region are different form those at fully developing region, we estimated all statistics in the region of fully developing mixing layer and omitted them in the region of $x < 0.6$. Although θ of the particle-laden cases (RUNs II–IV) are generally thin compared to the particle-free case (RUN I), their increase rates in the downstream region of $x > 3$ suddenly become large. This behavior is remarkable for smaller τ_P/τ_K, and agrees well with the above observation of the spanwise coherent vortices (Fig. 2).

Fig. 4 shows the vertical distributions of time-averaged particle volume fraction, ϕ_v/ϕ_{v0}, and streamwise velocity, $\overline{U}$, for RUNs I–IV at the upstream and downstream stations of $x = 0.6$ and 5.0. The time-averaged particle volume fraction, ϕ_v, is normalized by that of the inlet particle-laden (upper) side, ϕ_{v0}. The vertical distance, y, is normalized by using the momentum thickness, θ, and $y_{0.5}$, which is the vertical location of $(\overline{U} - U_l)/\Delta U = 0.5$. Although ϕ_v/ϕ_{v0} for all cases has peaks on the upper side and decreases to zero as approaching the lower side, the effect of τ_P/τ_K on the maximum values and the decreasing rates at the upstream and downstream stations are significantly different. That is, as τ_P/τ_K decreases, the peak value and decreasing rate of ϕ_v/ϕ_{v0} become greater at the upstream station of $x = 0.6$ but smaller at the downstream station of $x = 5.0$. The reason is considered as follows. The particles with smaller τ_P/τ_K are easily affected by the coherent vortices generated around the central interface because of smaller particle response time. Therefore, although the larger particles monotonically penetrate the coherent vortices, the small particles are pushed to the upper side by the primitive small-scale coherent vortices in the upstream region and carried to the lower side by the relatively developing large-scale coherent vortices in the downstream region where the centrifugal effect becomes strong. Conversely, as discussed later in detail, the particles with smaller τ_P/τ_K clearly affect the flow characteristics. Furthermore, the interesting thing is that in Fig. 4 unlike the behaviors of particle dispersion and coherent vortices, that of normalized time-averaged streamwise velocity is not changed by the

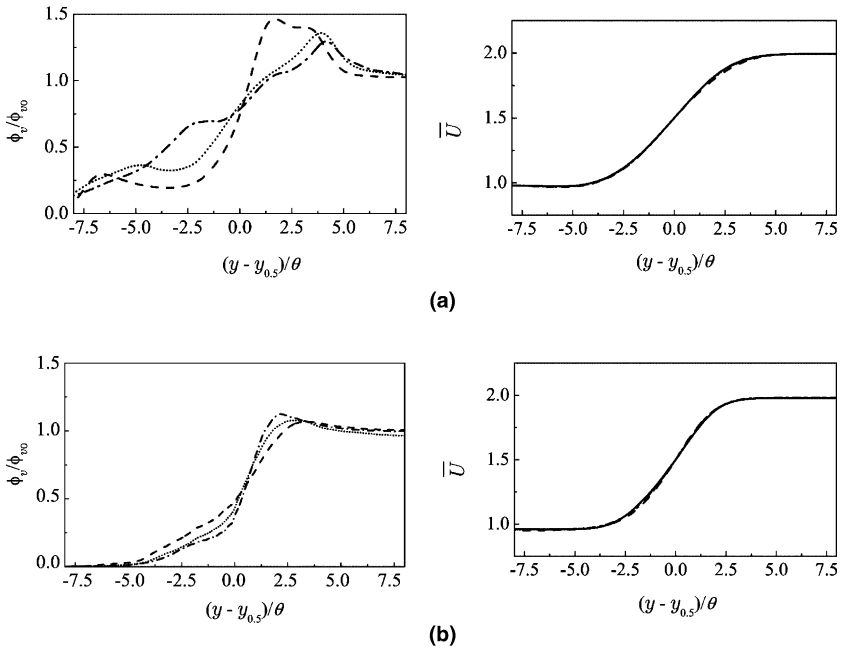

Fig. 4. Vertical distributions of time-averaged particle volume fraction, ϕ_v/ϕ_{v0}, and streamwise velocity, $\overline{U}$: (a) $x = 0.6$ and (b) $x = 5.0$. Symbols as in Fig. 3.

laden particles. The vertical distributions of $\overline{U}$ for all cases (RUNs I–IV) almost correspond to each other.

Fig. 5 shows the streamwise distributions of streamwise, vertical and spanwise turbulent intensities, $\overline{u^2}$, $\overline{v^2}$ and $\overline{w^2}$, respectively, at $y = y_{0.5}$. The experimental results of particle-free flow obtained by Michioka (2001) are plotted by black circles (●) in these figures. The Reynolds number in the experiment is 8000, which is almost identical to that of the present DNS ($Re = 8333$). The values of $\overline{u^2}$ and $\overline{v^2}$ for the particle-free flow (RUN I) obtained by the present DNS are in good agreement with the experimental values, which indicates the validity of the present DNS. It is found that the laden particles consistently depress the turbulent intensities in the upstream region of the mixing layer, whereas the effect of laden-particles on the turbulent intensities in the downstream region is varied with τ_P/τ_K. In the downstream region, $\overline{u^2}$ and $\overline{v^2}$ increase and become larger than those for the particle-free case (RUN I) as τ_P/τ_K decreases (see the profiles of RUNs II and III). These $\overline{u^2}$ and $\overline{v^2}$ behaviors are considered to be dominated by the behavior of the coherent vortices described above (the laden particles delay the development of the coherent vortices upstream but enhance it downstream). On the other hand, $\overline{w^2}$ is still depressed in the downstream region because the number of the ribs in the braid regions is decreased by loaded particles (the figure is not shown here). Though $\overline{u^2}$, $\overline{v^2}$ and $\overline{w^2}$ behaviors under the condition of $\tau_P/\tau_K > 1$ are not discussed in detail and figures are not shown here, we actually conducted a similar computation for larger particles with $\tau_P/\tau_K = 1.85$ and found that $\overline{u^2}$, $\overline{v^2}$ and $\overline{w^2}$ became much smaller than those for the $\tau_P/\tau_K = 0.5$ case (RUN IV). This trend is similar to the results of linear stability analysis of the mixing layer, in which particles of $\tau_P/\tau_K > 1.0$ are uniformly loaded in both low and high speed sides (Dimas and Kiger, 1998).

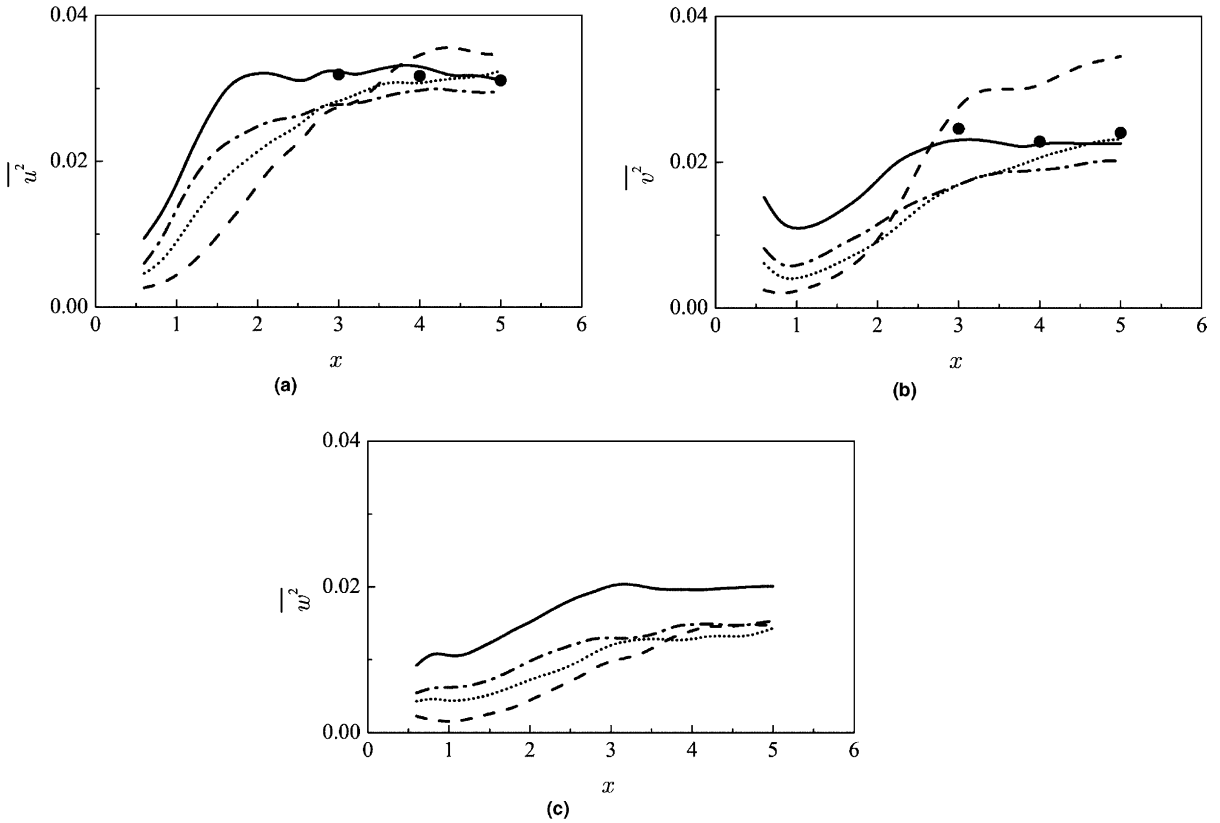

Fig. 5. Streamwise distributions of turbulent intensities for: (a) streamwise; (b) vertical and (c) spanwise velocity fluctuations, $\overline{u^2}, \overline{v^2}$ and $\overline{w^2}$, at $y = y_{0.5}$: (———) RUN I; (– – – –) RUN II; (·····) RUN III and (—· —· —) RUN IV; (●) measurement by Michioka (2001).

The power spectra of streamwise, vertical and spanwise velocity fluctuations at the downstream station of $x = 5.0$, $y = y_{0.5}$ are shown in Fig. 6. Due to the laden particles, the spanwise turbulent motions are depressed in the whole-scale regions, but for the streamwise and vertical components, the large-scale turbulent motions increase and small-scale turbulent motions decrease. Also, it was observed that in the upstream region, the turbulent motions of all three components are less for the particle-laden cases than that for the particle-free case (the figures are not shown here). Hence, it can be said that regardless of the coherent or non-coherent motion, the laden particles tend to suppress the small-scale turbulent motions and enhance the large-scale turbulent motions in the mixing layer. Consequently, in the downstream region, the large-scale coherent motions are enlarged, but the small-scale turbulent fluctuations in the coherent motions disappear. The high intensities of $\overline{u^2}$ and $\overline{v^2}$ in the downstream region are considered to be caused by the large-scale turbulent motions, which correspond to the spanwise coherent vortices. In addition, since the small-scale motions are decreased, the coherent spanwise vortices become clear downstream, as shown in Fig. 2. As a result, the smaller particles laden on the upper side (see Fig. 4(a)) act to suppress the growth of the primitive small-scale coherent vortices in the upstream region by accumulating only on the upper circumference of the coherent vortices, whereas they contrarily

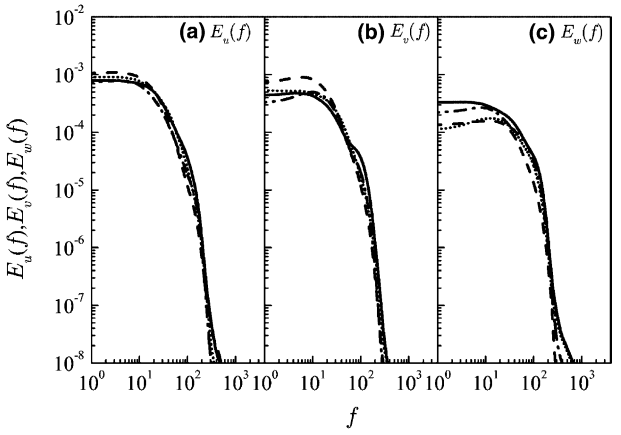

Fig. 6. Power spectra of: (a) streamwise; (b) vertical and (c) spanwise velocity fluctuations at $x = 5.0$. Symbols as in Fig. 3.

enhance the growth of the relatively developing large-scale coherent vortices in the downstream region because the downstream large-scale coherent vortices transport the smaller particles to the lower side (see Fig. 4(b)) and this promotes the amplitude of the vortices.

The above results are different from the previous DNS results (Ahmed and Elghobashi, 2000; Druzhinin, 2001) for homogeneous flows, in which the turbulence intensities are supposed to be always enhanced by the comparable laden particles. Druzhinin (2001), who performed the two-way coupled DNS of isotropic turbulence under the condition of $\tau_P < \tau_K$, stated that the enhancement of the kinetic energy (turbulent intensities) in the isotropic turbulence is caused by the fact that the laden particles add energy to fluid. To clarify the difference in the turbulent modulation mechanism between homogeneous and inhomogeneous flows, the transport equation for the turbulent intensities is introduced. This equation can be derived by multiplying Eq. (2) by u_j and is time-averaged,

$$\frac{\mathrm{D}\overline{u_i^2}}{\mathrm{D}t} = P_i + \Pi_i + \varepsilon_i + \phi_i, \tag{23}$$

where P_i is turbulence production by mean shear, Π_i is pressure–strain correlation, ε_i is energy dissipation and ϕ_i is energy exchange due to the particles drag force. The viscous diffusion was omitted in Eq. (23) because it is negligibly related to the modification of turbulent intensities. These terms are expressed as

$$P_i = -2\overline{u_i u_k}\frac{\partial \overline{U_i}}{\partial x_k}, \tag{24}$$

$$\Pi_i = 2\overline{p\frac{\partial u_i}{\partial x_i}}, \tag{25}$$

$$\varepsilon_i = -\frac{2}{Re}\overline{\frac{\partial u_i}{\partial x_k}\frac{\partial u_i}{\partial x_k}}, \tag{26}$$

$$\phi_i = 2u_i \Psi_{u_i}. \tag{27}$$

The energy exchange between fluid and particles, as mentioned before, is often discussed using the terms, ϕ_1, ϕ_2 and ϕ_3, in Eq. (23), because the turbulent intensities, $\overline{u^2}$, $\overline{v^2}$ and $\overline{w^2}$, are directly affected through these terms. Fig. 7 shows the streamwise distributions of ϕ_1, ϕ_2, and ϕ_3 at $y = y_{0.5}$. Here, the positive and negative values of ϕ_i mean that the laden particles act to increase and decrease the turbulent intensities, respectively. Although ϕ_i for all three components mostly indicate a negative or zero value, ϕ_1 for smaller τ_P/τ_K tend to increase and become positive as the streamwise distance from the inlet, x, increases. The trend is most evident for the smallest τ_P/τ_K (RUN II), and is significantly different from that in the isotropic turbulence where ϕ_i indicates a positive value (Druzhinin, 2001). This means that the laden particles with small τ_P/τ_K enhance the streamwise turbulent intensity, $\overline{u^2}$, downstream, which seems to generally agree with the $\overline{u^2}$ behavior in Fig. 5 [$\overline{u^2}$ for the small τ_P/τ_K (RUNs II and III) becomes greater than that for the particle-free case (RUN I)]. However, the profile of ϕ_1 cannot explain the behavior of $\overline{u^2}$ in detail. For the smallest τ_P/τ_K (RUN II), the value of $\overline{u^2}$ remains lower than that for the particle-free case (RUN I) in the upstream region of $x = 3.0$, even though ϕ_1 changes its sign from negative to positive at an early streamwise station less than $x = 1.0$. Moreover, the profiles of ϕ_2 and $\overline{v^2}$ are not correlated to each other [while $\overline{v^2}$ for the smaller τ_P/τ_K (RUNs II and III) goes beyond that for the particle-free case (RUN I) downstream, ϕ_2 remains negative]. These facts suggest that unlike in the case of isotropic turbulence (Druzhinin, 2001), the turbulent modulation owing to laden particles in the mixing layer cannot be explained solely by the energy exchange between fluid and particles.

Figs. 8 and 9 show the streamwise distributions of the turbulence production by mean shear, P_1, and the pressure-strain correlation, Π_i, at $y = y_{0.5}$. Here, P_2 and P_3 were not shown because they are very small compared to P_1. Usually, in the mixing layer flows, the mean shear produces the streamwise turbulent intensity, $\overline{u^2}$, through P_1 and a part of this streamwise turbulent energy is transferred to the vertical and spanwise turbulent intensities, $\overline{v^2}$ and $\overline{w^2}$, through Π_i due to the negative Π_1 and positive Π_2 and Π_3. This energy transfer also occurs in the particle-laden mixing layer flows. However, the laden particles act to delay the P_1 evolution, increase Π_2, and decrease

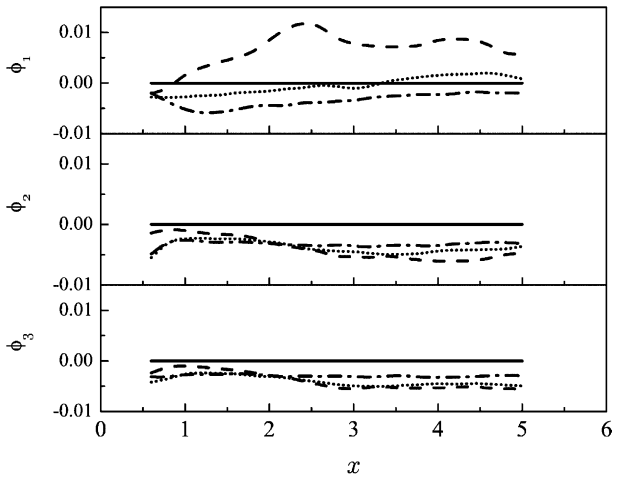

Fig. 7. Streamwise distributions of energy exchange between fluid and particles, ϕ_1,ϕ_2 and ϕ_3, at $y = y_{0.5}$. Symbols as in Fig. 3.

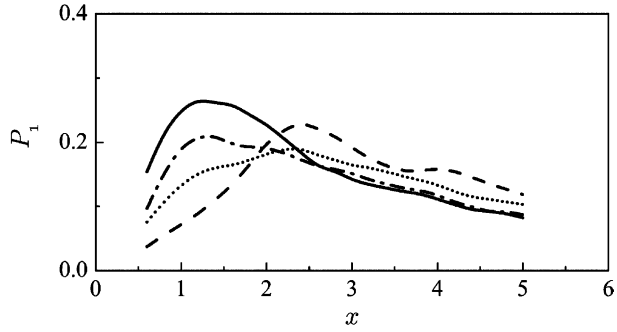

Fig. 8. Streamwise distributions of turbulent production by mean shear, P_1, at $y = y_{0.5}$. Symbols as in Fig. 3.

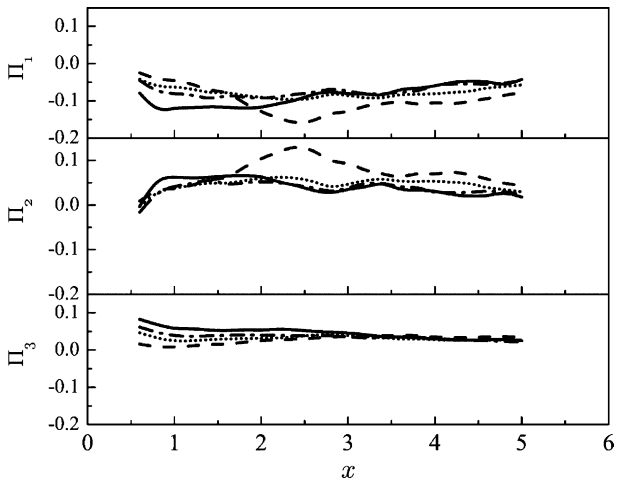

Fig. 9. Streamwise distributions of pressure–strain correlation, Π_1, Π_2 and Π_3, at $y = y_{0.5}$. Symbols as in Fig. 3.

Π_3 (these trends are significant for the particles with smaller τ_P/τ_K). As a result, the turbulent intensities in the upstream region decrease, and the streamwise and vertical turbulent intensities in the downstream region increase, as shown in Fig. 5 (see RUNs II and III). In particular, Π_2 for the smallest τ_P/τ_K (RUN II) becomes much greater than those for other cases in the region of $x > 2.0$, which may be the reason for the rapid increase of $\overline{v^2}$ downstream. Thus, the turbulent modulation owing to the laden particles in the mixing layer is dominated by the turbulence production by mean shear and the pressure–strain correlation, not by the energy exchange between fluid and particles. Likewise, Ahmed and Elghobashi (2000) previously conducted the two-way coupled DNS of turbulent homogeneous shear flows with dispersed particles and showed that the enhancement of the turbulent intensities in the fields is mainly attributed to the energy production by the mean shear. However, in the particle-laden mixing layer, since the energy production by the mean shear dramatically varies with the streamwise distance, the effect of particles on the turbulent intensities also dramatically varies with the streamwise distance.

Fig. 10 shows the streamwise distributions of the energy dissipation, ε_1, ε_2 and ε_3, at $y = y_{0.5}$. The absolute values of ε_1,ε_2 and ε_3 for the particle-laden cases (RUNs II–IV) are less than those for the particle-free case (RUN I), and they monotonically approach zero as τ_P/τ_K decreases. Ahmed and Elghobashi (2000) stated that the modification of ε_i is proportional to that of turbulence kinetic energy (turbulent intensity). However, such a relation cannot be seen in the present study (compare Fig. 10 with Fig. 5). This is because the enhancement of $\overline{u^2}$ and $\overline{v^2}$ is mainly attributed to the large-scale motions produced by mean shear, whereas the small-scale structure, by which ε_1 and ε_2 are strongly affected, becomes small as shown in Fig. 6.

3.2. Effect of particle response time on chemical species' diffusion and reaction (zero gravity condition)

The effects of particle response time, τ_P, on chemical species' diffusion and reaction are discussed using the results of RUNs I–IV under the zero gravity condition.

Fig. 11 shows the streamwise distributions of the amount of chemical product P, P_T, normalized by that for the particle-free case (RUN I) at $x = 5.0$, $P_{T,(x=5)}$. Here, P_T is given by integrating the mean chemical product along the vertical axis

$$P_T = \int_{-0.5}^{0.5} \overline{\Gamma_P}(y)\mathrm{d}y. \tag{28}$$

The values of P_T for the particle-laden cases (RUNs II–IV) are found to be less than that for the particle-free case (RUN I) in the whole region. Also, as τ_P/τ_K decreases, the magnitude of P_T decreases in the upstream region but the increase rate in the downstream region becomes slightly large. What should be noted here is that, in spite of the remarkable increments of the turbulent intensities owing to the laden particles in the downstream region [see Fig. 5; a similar trend also appears for the mean-squared values of concentration fluctuations of chemical species A (Fig. 12)], the values of P_T for the particle-laden cases (RUNs II–IV) do not exceed that for

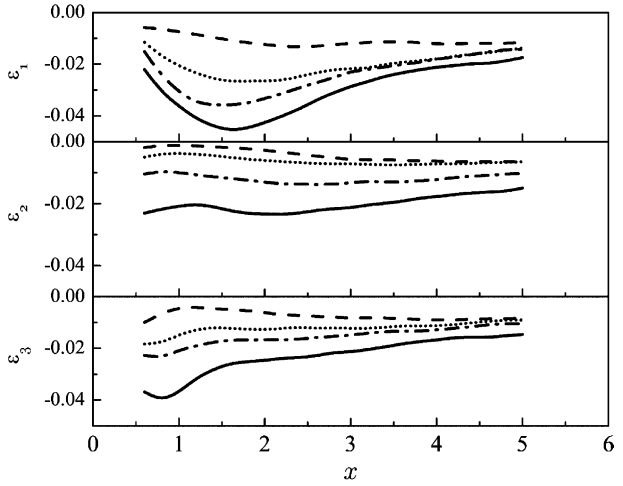

Fig. 10. Streamwise distributions of energy dissipation, ε_1, ε_2 and ε_3, at $y = y_{0.5}$. Symbols as in Fig. 3.

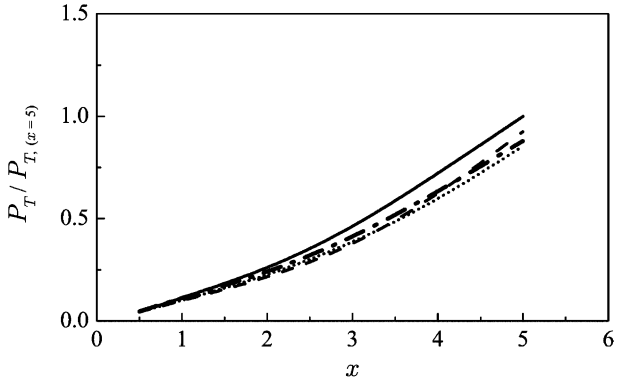

Fig. 11. Streamwise distributions of amount of chemical product P, P_{T}, at $y = y_{0.5}$. Symbols as in Fig. 3.

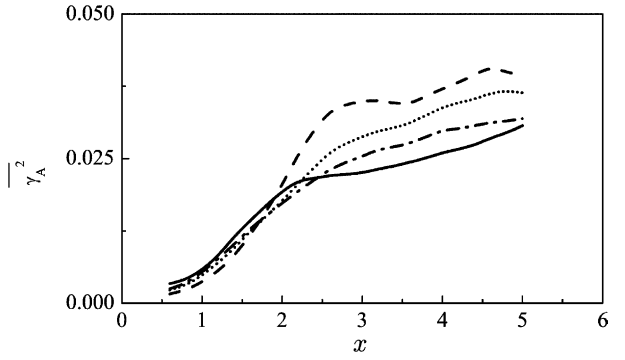

Fig. 12. Streamwise distributions of mean-squared values of concentration fluctuations of chemical species A, $\overline{\gamma_{\mathrm{A}}^2}$, at $y = y_{0.5}$. Symbols as in Fig. 3.

the particle-free case (RUN I). As mentioned before, the laden particles tend to suppress the small-scale turbulent motions and enhance the large-scale turbulent motions in the mixing layer. Therefore, it is considered that since the small-scale turbulence in the coherent vortices, which promotes a chemical reaction, is suppressed by the laden particles in the whole region, the chemical product is decreased overall (although the figure is not shown here, we conducted the DNS for other Damköhler numbers and verified that the above behaviors were similarly observed).

Comparison of the streamwise distributions between the turbulent intensities, $\overline{u_i^2}$, (Fig. 5) and the mean-squared values of concentration fluctuations of chemical species A, $\overline{\gamma_{\mathrm{A}}^2}$, (Fig. 12) shows that the increment of $\overline{\gamma_{\mathrm{A}}^2}$ owing to the laden particles in the downstream region is much more remarkable than that of $\overline{u_i^2}$. To understand this difference, the transport equation for $\overline{\gamma_{\mathrm{A}}^2}$

$$\frac{\mathrm{D}\overline{\gamma_{\mathrm{A}}^2}}{\mathrm{D}t} = \frac{-2\overline{v\gamma_{\mathrm{A}}}\frac{\partial\overline{\Gamma_{\mathrm{A}}}}{\partial y}}{P_{\gamma_{\mathrm{A}}^2}} + \frac{1}{ReSc}\frac{\partial^2\overline{\gamma_{\mathrm{A}}^2}}{\partial x_j \partial x_j} - \frac{2}{ReSc}\overline{\frac{\partial\gamma_{\mathrm{A}}}{\partial x_j}\frac{\partial\gamma_{\mathrm{A}}}{\partial x_j}} - \frac{\partial}{\partial x_j}\left(\overline{\gamma_{\mathrm{A}}^2 u_j}\right) + Da\left(\overline{\gamma_{\mathrm{A}}^2}\overline{\Gamma_{\mathrm{B}}} + \overline{\gamma_{\mathrm{A}}\gamma_{\mathrm{B}}}\overline{\Gamma_{\mathrm{A}}} + \overline{\gamma_{\mathrm{A}}^2\gamma_{\mathrm{B}}}\right), \tag{29}$$

is considered. Here, $P_{\overline{\gamma_A^2}}$ is scalar-variance production by mean concentration distribution. Usually, the $\overline{\gamma_A^2}$ behavior is mainly governed by $P_{\overline{\gamma_A^2}}$, so that their streamwise distributions at $y = y_{0.5}$ are as shown in Fig. 13. Similar to the turbulence production by mean shear, P_1, [see Eq. (23) and Fig. 8], the values of $P_{\overline{\gamma_A^2}}$ for the particle-laden cases (RUNs II–IV) are smaller than that for the particle-free case (RUN I) in the upstream region, but they become larger in the downstream region. Hence, the laden particles are found to have comparable influences on P_1 and $P_{\overline{\gamma_A^2}}$. The significant difference from the transport equation of $\overline{u_i^2}$ is that the transport equation of $\overline{\gamma_A^2}$ does not contain the direct interaction term with the particles. As shown in Fig. 7, in the upstream region the energy exchange between fluid and particles tends to be totally negative, which acts to depress $\overline{u_i^2}$ for the particle-laden case. On the other hand, since the $\overline{\gamma_A^2}$ behavior is not directly affected by the particles, $\overline{\gamma_A^2}$ is not decreased. Thus, whether there exists an interaction term with the particles or not results in the difference in the modification behavior between the turbulent intensities and squared values of concentration fluctuations. The other terms in Eq. (29) were not shown because they are negligibly related to the modification of $\overline{\gamma_A^2}$.

3.3. Effects of particle volume fraction on turbulence and chemical species' diffusion and reaction (zero gravity condition)

The effects of initial particle volume fraction, ϕ_{v0}, on turbulence and chemical species' diffusion and reaction are studied under the zero gravity condition using RUNs I, II, V and VI. As listed in Table 1, the initial particle volume fractions of RUNs II, V and VI range from 1.68×10^{-5} to 1.07×10^{-3} with the same non-dimensional particle response time of $\tau_P/\tau_K = 0.12$.

Figs. 14 and 15 show the effects of the initial particle volume fraction, ϕ_{v0}, on the turbulent intensities, $\overline{u^2}, \overline{v^2}$ and $\overline{w^2}$ and mean-squared values of concentration fluctuations of chemical species A, $\overline{\gamma_A^2}$, at $y = y_{0.5}$. In general, the deviations of profiles for the particle-laden cases (RUNs II, V and VI) from those of the particles-free case (RUN I) become significant as ϕ_{V0} increases. Although the figures are not shown, same behaviors were observed in the streamwise distributions of the momentum thickness, θ, and amount of the chemical product P, P_t. Namely, these properties become less in the upstream region, and the increase rates become slightly greater in the downstream region. The trends of these properties with ϕ_{V0} are similar to those with the particle response time, τ_P/τ_K (strictly speaking, similar to those with the inverse number of τ_P/τ_K), as

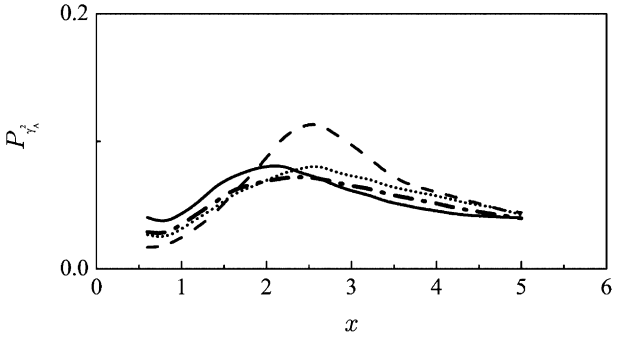

Fig. 13. Streamwise distributions of scalar-variance production, $P_{\overline{\gamma_A^2}}$, at $y = y_{0.5}$. Symbols as in Fig. 3.

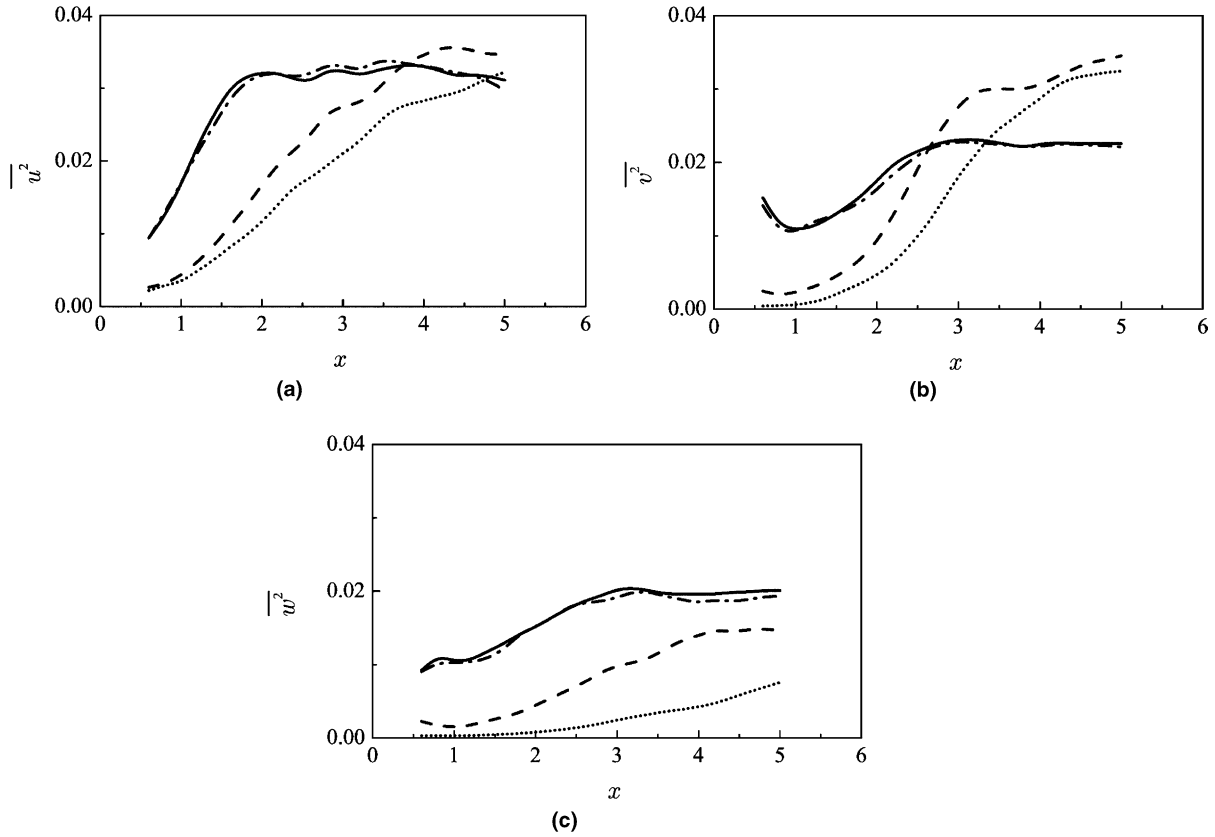

Fig. 14. Streamwise distributions of turbulent intensities for: (a) streamwise; (b) vertical and (c) spanwise velocity fluctuations, $\overline{u^2}$, $\overline{v^2}$ and $\overline{w^2}$, at $y = y_{0.5}$. θ: (———) RUN I; (– – – –) RUN II; (–·–·–) RUN V and (·····) RUN VI.

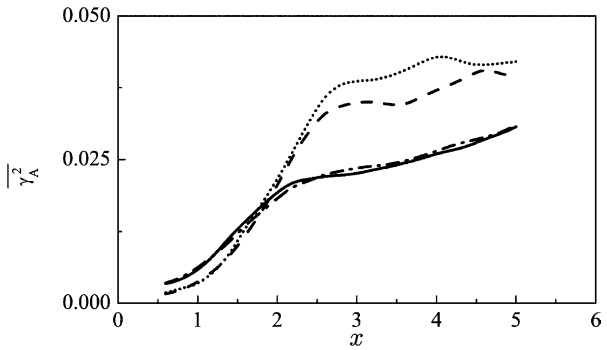

Fig. 15. Streamwise distribution of mean-squared values of concentration fluctuations of chemical species A, $\overline{\gamma_A^2}$, at $y = y_{0.5}$. Symbols as in Fig. 14.

mentioned before (see Figs. 5 and 12). It was also observed that more particles tend to gather at the circumference of coherent vortices generated around the central interface with increasing ϕ_{v0},

and that the development of coherent vortices is further delayed and they become large downstream (figures are not shown). Therefore, it can be concluded that, for the small particles with $\tau_P/\tau_K = 0.12$, which easily accumulate at the circumference of coherent vortices, the increment of the number of particles encourages the suppression of growth of small-scale turbulent motions in the upstream region and the enhancement of growth of large-scale turbulent motions (coherent vortices) in the downstream region of the mixing layer.

3.4. Effect of finite gravity on particles on turbulence and chemical species' diffusion and reaction

The effects of the finite gravity on particles on turbulence and chemical species' diffusion and reaction are discussed by comparing the results for the zero gravity condition (RUNs II–IV) with those for the finite gravity condition (RUNs IIG–IVG) (see Table 1). The initial particle volume fractions on the high-speed side for all cases are the same ($\phi_{V0} = 2.62 \times 10^{-4}$), and their particle response times are varied ($\tau_P/\tau_K = 0.12-0.50$). The finite gravity is imposed in y direction. The terminal velocities of these particles for RUNs IIG–IVG, v_t, are 9.02×10^{-3}, 2.32×10^{-2} and 5.68×10^{-2}, respectively.

Fig. 16 shows the instantaneous particle distributions superimposed on spanwise vorticity in (x,y)-plane for the finite-gravity-imposed cases (RUNs IIG–IVG). Compared to the zero-gravity-imposed cases (RUNs II–IV) the particles in the presence of the finite gravity (RUNs

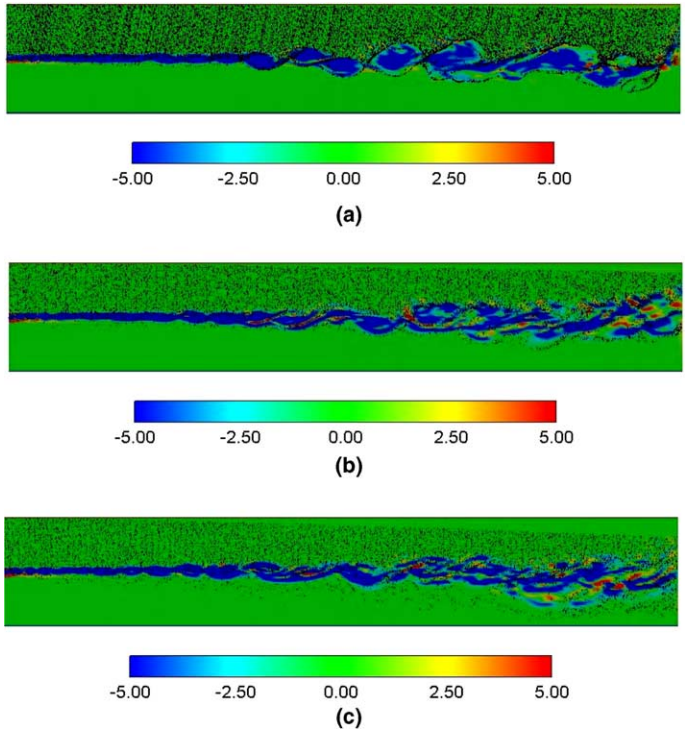

Fig. 16. Instantaneous particle distributions superimposed on spanwise vorticities in (x,y)-plane for: (a) RUN IIG, (b) RUN IIIG, and (c) RUN IVG in the presence of finite gravity. The gray plots represent particles.

IIG–IVG) distribute on the lower side as going further downstream, and this effect is significant for larger τ_P/τ_K. It is also found that while the particles with the smallest τ_P/τ_K (RUN IIG) accumulate near the circumference of the coherent vortices as they do for the zero-gravity-imposed case (RUN II) (see Fig. 2), many of the particles with larger τ_P/τ_K (RUNs IIIG and IVG) penetrate the spanwise coherent vortices owing to the larger terminal velocity. These behaviors are verified in Fig. 17(a), which shows the vertical distributions of the particle volume fraction, ϕ_v/ϕ_{v0}, at the streamwise station of $x = 5.0$. In spite of the difference in the particle distribution, the time-averaged streamwise velocities, $\overline{U}$, are almost identical irrespective of the presence or absence of gravity [see Fig. 17(b)]. These facts mean that the presence of the finite gravity affects the particle behavior, but negligibly affects the time-averaged fluid behavior in the particle-laden mixing layer.

Fig. 18 shows the streamwise distributions of the streamwise, vertical and spanwise turbulent intensities, $\overline{u^2}, \overline{v^2}$ and $\overline{w^2}$, in the presence of finite gravity at $y = y_{0.5}$. While $\overline{u^2}, \overline{v^2}$ and $\overline{w^2}$ for the smaller τ_P/τ_K (RUNs IIG and IIIG) are almost identical to those for the zero gravity condition (RUNs II and III), for the largest τ_P/τ_K (RUN IVG) they become smaller than those for the zero gravity condition (RUN IV) particularly in the downstream region. This can be explained by considering the variations of the turbulent production by mean shear, P_1, and the energy exchange between fluid and particles, ϕ_1,ϕ_2 and ϕ_3. Figs. 19 and 20 show the comparisons of the streamwise distributions of P_1, ϕ_1,ϕ_2 and ϕ_3 at $y = y_{0.5}$ between the zero- and finite-gravity-imposed cases for the largest τ_P/τ_K (RUNs IV and IVG, $\tau_P/\tau_K = 0.50$). The profile of P_1 for the finite-gravity-imposed case (RUN IVG) nearly corresponds to the zero-gravity-imposed case (RUN IV), which indicates that the effect of the presence of gravity on P_1 is quite small. On the other hand, the values of ϕ_1, ϕ_2 and ϕ_3 are found to be markedly decreased by the presence of gravity. Thus, the particles with larger particle response time tend to depress the turbulent intensities by increasing the energy transfer from fluid to particles in the presence of finite gravity.

The streamwise distributions of the mean-squared values of concentration fluctuations of chemical species A, $\overline{\gamma_A^2}$, at $y = y_{0.5}$ are shown in Fig. 21. The profiles of $\overline{\gamma_A^2}$ for the finite-gravity-imposed cases (RUNs IIG–IVG) are found to be nearly identical to those for the zero-gravity-imposed

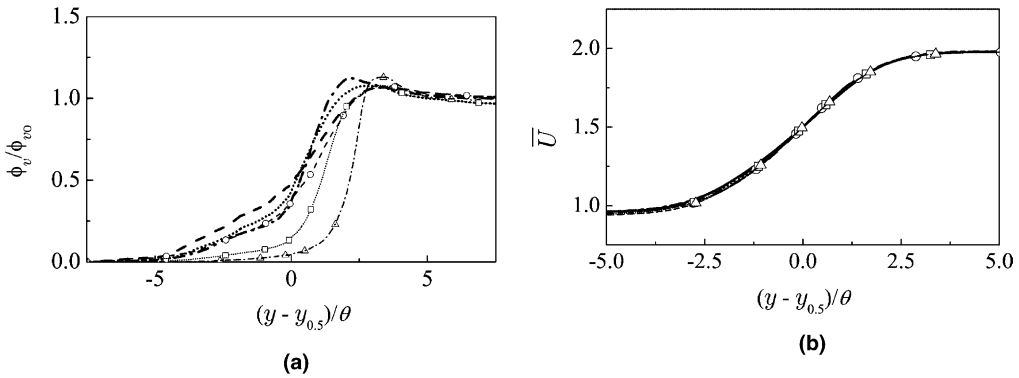

Fig. 17. Vertical distributions of time-averaged: (a) particle volume fraction,ϕ_v/ϕ_{v0} and (b) streamwise velocity, $\overline{U}$, in the presence of finite gravity at $x = 5.0$: (– – – –) RUN II; (·····) RUN III; (— · —) RUN IV; (○ – ○) RUN IIG; (□·····□) RUN IIIG; (△ · – · △) RUN IVG.

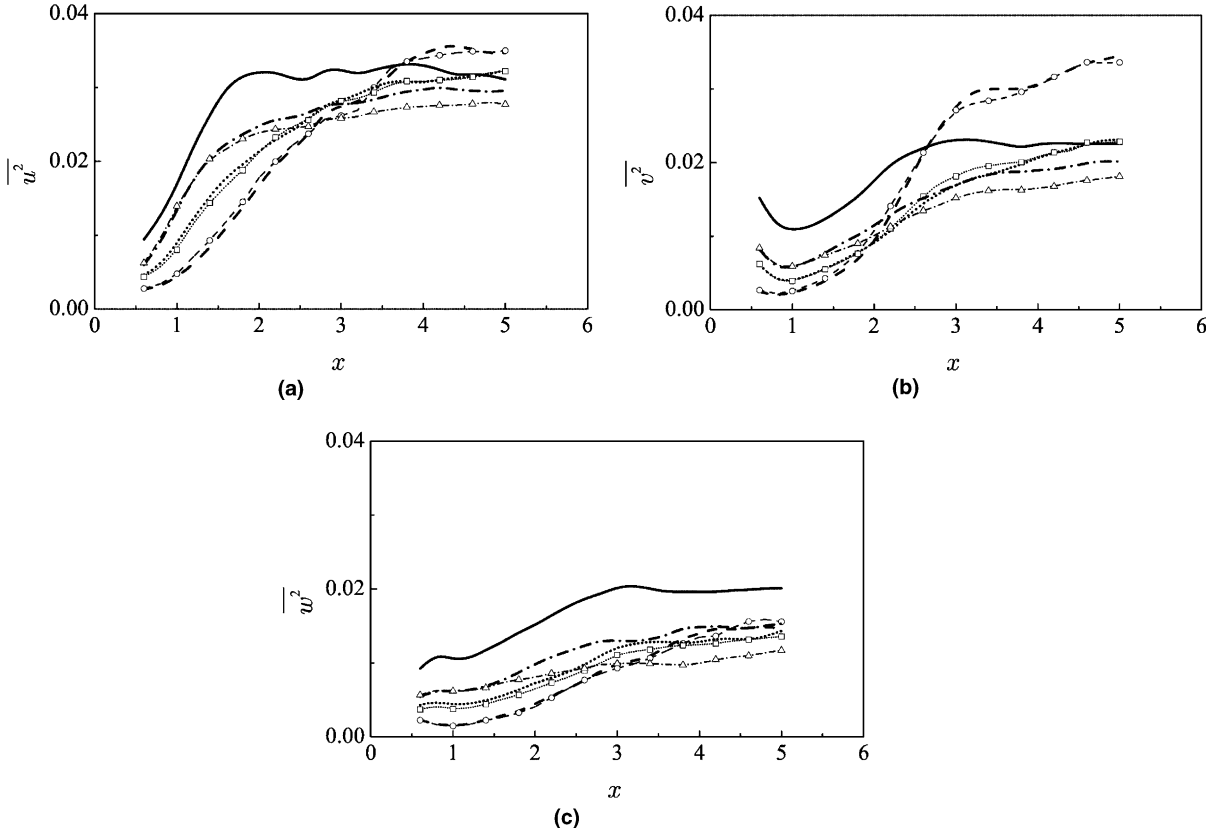

Fig. 18. Streamwise distributions of turbulent intensities for: (a) streamwise; (b) vertical and (c) spanwise velocity fluctuations, $\overline{u^2}$, $\overline{v^2}$and $\overline{w^2}$, in the presence of finite gravity at $y = y_{0.5}$: (———) RUN I; (– – – –) RUN II; (·····) RUN III; (— · —) RUN IV; (○ – ○) RUN IIG; (□·····□) RUN IIIG and (△ – · – △) RUN IVG.

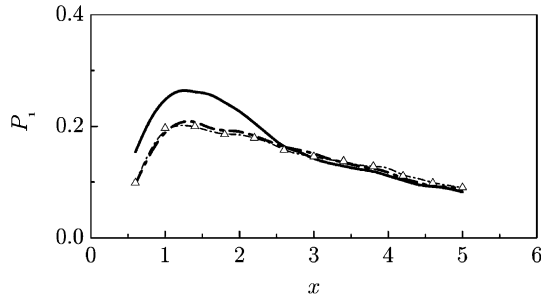

Fig. 19. Streamwise distributions of turbulent production by mean shear, P_1, in the presence of finite gravity at $y_{0.5}$: (———) RUN I; (— · —) RUN IV and (△ – · – △) RUN IVG.

cases (RUNs II–IV), even for the largest τ_P/τ_K. Also, the amounts of chemical product P, P_T, for finite-gravity-imposed cases were also equal to those for the zero-gravity-imposed cases (the

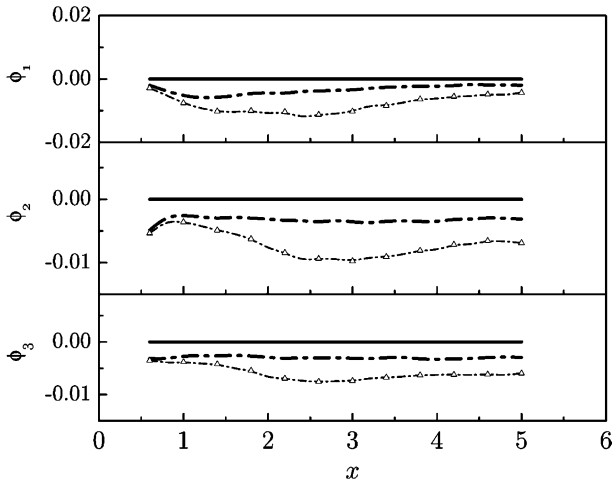

Fig. 20. Streamwise distributions of energy exchange between fluid and particles, ϕ_1, ϕ_2 and ϕ_3, in the presence of finite gravity at $y = y_{0.5}$. Symbols as in Fig. 19.

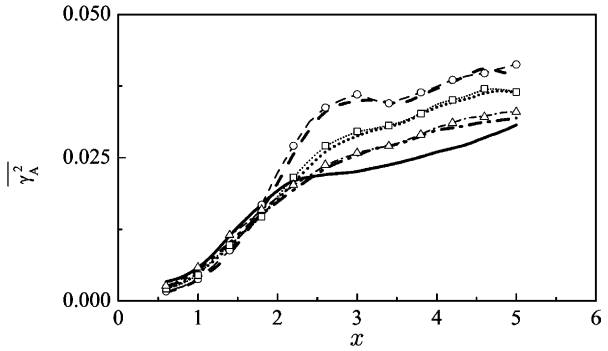

Fig. 21. Streamwise distributions of mean-squared values of concentration fluctuations of chemical species A, $\overline{\gamma_A^2}$, in the presence of finite gravity at $y = y_{0.5}$. Symbols as in Fig. 18.

figures are not shown here). These results show that the finite gravity acting on the laden particles has little influence on the behaviors of $\overline{\gamma_A^2}$ and P_T in the particle-laden mixing layer. The reason for this is considered to be that the concentration fluctuation of chemical species is not directly affected by the particles themselves, as shown in Eq. (29), unlike the turbulent intensities, in whose transport equation there exists the fluid-particle energy exchange term.

4. Conclusions

A direct numerical simulation (DNS) was applied to a particle-laden mixing layer with a chemical reaction, and effects of particles on the turbulence, diffusion of chemical species and amount of chemical product in both zero and finite gravity cases were investigated. The unreactive parti-

cles, whose response time, τ_P, was smaller than the Kolmogorov time scale, τ_K, $[\tau_P/\tau_K = O(10^{-1})]$, were uniformly injected into the high-speed side of the mixing layer, and all particle trajectories were individually pursued in a Lagrangian manner. Two reactive chemical species were separately introduced through different sides, and a second-order, irreversible and isothermal reaction between them was assumed to take place in the region along the interface. The main results from this study can be summarized as follows.

The laden particles generally depress turbulent intensities on the centerline in the mixing layer, but they begin to enhance the streamwise and vertical turbulent intensities downstream as the particle response time decreases provided the inlet particle volume fraction is fixed. This modulation is attributed to the fact that the small particles with small particle response time easily accumulate at the circumference of coherent vortices generated around the central interface and act to suppress the growth of primitive small-scale coherent vortices upstream but enhance that of relatively developing large-scale ones downstream (the increment of particle volume fraction promotes these effects). Thus, the laden particles with $\tau_P/\tau_K = O(10^{-1})$ have two effects of depressing or enhancing turbulent intensities, and this behavior is different from those of particle-laden turbulent homogeneous flows, in which a comparable loaded particle always enhances the turbulent intensities.

Due to the laden particles, the mean-squared value of the concentration fluctuation of chemical species is also depressed in the upstream region, but it is enhanced in the downstream region regardless of the inlet particle volume fraction and particle response time. This trend is different from that of the turbulent intensities, which is enhanced only by the smaller particles in the downstream region. The difference is caused by the fact that the concentration fluctuation of chemical species is not directly affected by particles. Moreover, the chemical product is decreased overall, because the small-scale turbulence in the coherent vortices, which promotes the chemical reaction, is suppressed by the laden particles in the whole region. Furthermore, the presence of the finite gravity acts to depress the turbulent intensities in the particle-laden mixing layer, but its effects on chemical species' diffusion and reaction are quite small.

References

Ahmed, A.M., Elghobashi, S., 2000. On the mechanisms of modifying the structure of turbulent homogeneous shear flows by dispersed particles. Phys. Fluids 12, 2906–2930.

Book, D.L., Boris, J.P., Hain, K., 1975. Flux-corrected transport. II: Generalizations of the method. J. Comput. Phys. 18, 248–283.

Boivin, M., Simonin, O., Squires, K.D., 1998. Direct numerical simulation of turbulence modulation by particles in isotropic turbulence. J. Fluid Mech. 375, 235–263.

Boris, J.P., Book, D.L., 1973. Flux-corrected transport. I. SHASTA, a fluid transport algorithm tha works. J. Comput. Phys. 11, 38–69.

Boris, J.P., Book, D.L., 1976. Flux-corrected transport. III: Minimal-error FCT algorithms. J. Comput. Phys. 20, 397–431.

Crowe, C.T., Sharma, M.P., Stock, D.E., 1977. The Particle-Source-in Cell (PSI-Cell) method for Gas-Droplet flows. Trans. ASME I: J. Fluids Engng. 6, 325–332.

Dimas, A.A., Kiger, K.T., 1998. Linear instability of a particle-laden mixing layer with a dynamic dispersed phase. Phys. Fluids 10, 2539–2557.

Druzhinin, O.A., 2001. The influence of particle inertia on the two-way coupling and modification of isotropic turbulence by microparticles. Phys. Fluids 13, 3738–3755.

Elghobashi, S., 1991. Particle-laden turbulent flows: direct simulation and closure models. Appl. Sci. Res. 48, 301–314.
Elghobashi, S., 1994. On predicting particle-laden turbulent flows. Appl. Sci. Res. 52, 309–329.
Elghobashi, S., Truesdell, G.C., 1993. On the two-way interaction between homogeneous turbulence and dispersed solid particles. I; Turbulence modification. Phys. Fluids A5, 1790–1801.
Fan, J., Zheng, Y., Yao, J., Cen, K., 2001. Direct simulation of particle dispersion in a three-dimensional temporal mixing layer. Proc. R. Soc. London A 457, 2151–2166.
Ferrante, A., Elghobashi, S., 2003. On the physical mechanisms of two-way coupling in particle-laden isotropic turbulence. Phys. Fluids 15, 315–329.
Ferziger, J.H., Peric, M., 2002. Computational Methods for Fluid Dynamics, third ed. Springer-Verlag.
Glaze, D.J., Frankel, S.H., 2000. Effect of dispersion characteristics on particle temperature in an idealized nonpremixed reacting jet. Int. J. Multiphase Flow 26, 609–633.
Hishida, K., Ando, A., Maeda, M., 1992. Experiments on particle dispersion in a turbulent mixing layer. Int. J. Multiphase Flow 18, 181–194.
Ishima, T., Hishida, K., Maeda, M., 1993. Effect of particle residence time on particle dispersion in a plane mixing layer. Trans. ASME I: J. Fluids Eng. 115, 751–759.
Kim, J., Moin, P., 1985. Application of a fractional-step method to incompressible Navier–Stokes equations. J. Comput. Phys. 59, 308–323.
Kurose, R., Komori, S., 1999. Drag and lift forces on a rotating sphere in a linear shear flow. J. Fluid Mech. 384, 183–206.
Kurose, R., Makino, H., 2003. Large eddy simulation of a solid-fuel jet flame. Combust. Flame 135, 1–16.
Ling, W., Chung, J.N., Troutt, R.T., Crowe, C.T., 1998. Direct numerical simulation of a three-dimensional temporal mixing layer with particle dispersion. J. Fluid Mech. 358, 61–85.
Mashayek, F., 2000. Numerical investigation of reacting droplets in homogeneous shear turbulence. J. Fluid Mech. 405, 1–36.
Mei, R., 1992. An approximate expression for the shear lift force on a spherical particle at finite Reynolds number. Int. J. Multiphase Flow 18, 145–147.
Meiburg, E., Wallner, E., Pagella, A., Riaz, A., Hartel, C., Necker, F., 2000. Vorticity dynamics of dilute two-way-coupled particle-laden mixng layers. J. Fluid Mech. 421, 185–227.
Michioka, T., 2001. Development of large eddy simulations of turbulent flows with a chemical reaction. Ph.D. Thesis, Department of Mechanical Engineering, Kyoto University (in Japanese).
Michioka, T., Sato, A., Sada, K., 2003. Large-eddy simulation for the tracer gas concentration fluctuation in atmospheric boundary layer. Trans. JSME Ser. B. 69, 868–875 (in Japanese).
Michioka, T., Komori, S., 2004. Large-eddy simulation of a turbulent reacting liquid flow. AIChE J. 50, 2705–2720.
Reveillon, J., Vervisch, L., 2000. Spray vaporization in nonpremixed turbulent combustion modeling: a single droplet model. Combust. Flame 121, 75–90.
Saffman, P.G., 1965. The lift on a small sphere in a slow shear flow. J. Fluid Mech. 22, 385–400.
Spalart, P.R., 1988. Direct simulation of a turbulent boundary layer up to $Re_\theta = 1410$. J. Fluid Mech. 187, 61–98.
Squires, K.D., Eaton, J.K., 1990. Particle response and turbulence modification in isotropic turbulence. Phys. Fluids A 2, 1191–1203.
Sundaram, S., Collins, L.R., 1999. A numerical study of the modulation of isotropic turbulence by suspended particles. J. Fluid Mech. 379, 105–143.
Wang, L., Maxey, M.R., 1993. Settling velocity and concentration distribution of heavy particles in homogeneous isotropic turbulence. J. Fluid Mech. 256, 27–68.
Yamamoto, Y., Potthoff, M., Tanaka, T., Kajishima, T., Tsuji, Y., 2001. Large-eddy simulation of turbulent gas–particle flow in a vertical channel: effect of considering inter-particle collisions. J. Fluid Mech. 442, 303–334.
Yang, Y., Chung, J.N., Troutt, T.R., Crow, C.T., 1990. The influence of particles on the spatial stability of two-phase mixing layers. Phys. Fluids A 2, 1839–1845.
Yonemura, S., Tanaka, T., Tsuji, Y., 1973. Cluster formation in gas–solid flow predicted by the DSMC method. In: Gas–Solid Flows. FED-Vol. 116, pp. 303–309.
Yuu, S., Umekage, T., Tabuchi, M., 1996. Direct numerical simulation for three-dimensional gas–solid two-phase jet using two-way method and experimental verification. JSME Int. J. Series B: Fluids Therm. Eng. 39, 230–245.